

Vision-Based Target Three-Dimensional Geolocation Using Unmanned Aerial Vehicles

Lele Zhang¹, Fang Deng¹, *Member, IEEE*, Jie Chen², *Senior Member, IEEE*, Yingcai Bi,
Swee King Phang³, *Member, IEEE*, Xudong Chen, and Ben M. Chen, *Fellow, IEEE*

Abstract—This paper develops a method of calculating the three-dimensional (3-D) coordinates of a target with image information taken from an unmanned aerial vehicle (UAV). Unlike the usual approaches to target geolocation that rely heavily on georeferenced terrain database or accurate attitude sensors, the contribution of the proposed method is to offset the constraints and also perform 3-D geolocation of the target based on the relative altitude between the aircraft and the target calculated using the stereo vision technique. Considering the poor performance of the yaw-angle measurement provided by the low-quality attitude sensors in the UAV, a novel vision-based 3-D geolocation method is designed. The proposed method is proven to be valid and practical via simulation results and actual flight experiments.

Index Terms—Altitude estimation, computer vision, target 3-D geolocation, unmanned aerial vehicle (UAV).

I. INTRODUCTION

UNMANNED aerial vehicles (UAVs) are increasingly being used for a wide variety of missions, such as surveillance, reconnaissance, and intelligence [1]–[4]. In most cases, a camera is one of the common sensors employed for UAVs to achieve high autonomy [5]. Today, we see many UAV applications strongly rely on the vision system, such as a vision-based autonomous cargo transfer [6], ground target following with a real-time embedded vision system [7], vision-based navigation strategy for the UAV to fly in a GPS-denied environment [8], motion estimation for multirotor UAVs by using only an off-board camera [9], and automatic detection for wind turbine blade surface cracks based on images taken by UAVs [10]. In particular,

an accurate and reliable vision-based target position estimation using an UAV is a fundamental issue for disaster monitoring, target tracking, and rescue mission. Generally speaking, it depends on accurate yaw-angle measurements and a known terrain map for providing altitude information of the target, so it is not suitable for the onboard low-quality attitude sensor and unknown environment. For this reason, this paper aims to solve the problem by using only vision to estimate the yaw-angle error and the altitude of the target, which is a challenge.

In recent years, researchers have paid much attention to target geolocation using visual cameras for the UAV system. Kaminer *et al.* [11], [12] showed that the vision-based tracking system could estimate the coordinates of a moving target in real time with a gimbal-stabilized camera, but an accurate georeferenced terrain database like the perspective view nascent technology system [13] is required to obtain the target's altitude. Barber *et al.* [14] discussed four techniques to reduce the localization error of a stationary target provided that a terrain map is available. Campbell *et al.* [15] developed a square-root estimator to determine the three-dimensional (3-D) location of both stationary and moving targets, however, the estimator needs a uniform distribution of bias uncertainties through a series of special experiments and so it is not easy to use in practical applications. Han *et al.* [16] provided a method to calculate the height of the UAV above a target using the computer vision, but this method assumes an accurate attitude-heading reference system (AHRS) mounted in the UAV. Pachter *et al.* [17] described a technique for mitigating AHRS's errors by taking multiple bearing measurements of the ground object of interest, it is strongly built upon the assumption that the ground object's elevation is known. The existing methods described previously place one or more requirements on the UAV systems and limit their fields of application.

In order to solve the problem, we develop a method of calculating the 3-D coordinates of a stationary or moving target with image information taken from an UAV, equipped with a low-quality AHRS. The method has none of the aforementioned requirements, and yet it yields an accurate estimate for the target location. This proposed vision-based geolocation method can be considered as an extension of the work reported in [17]. In that work, AHRS's heading-measurement bias can only be estimated using multiple bearing measurements of the ground object of interest (GOI) and linear regression [18], but the target's altitude has not been considered. In this paper, besides estimating the AHRS's yaw-angle measurement bias, the relative altitude between UAV and GOI is obtained as a

Manuscript received August 1, 2017; revised January 13, 2018; accepted February 5, 2018. Date of publication February 19, 2018; date of current version June 1, 2018. This work was supported in part by the National Natural Science Foundation of China under Grant U1613225, in part by the Beijing NOVA Program xx2016B027, and in part by China Scholarship Council. (*Corresponding author: Fang Deng.*)

L. Zhang, F. Deng, and J. Chen are with the Key Laboratory of Intelligent Control and Decision of Complex Systems, School of Automation, Beijing Institute of Technology, Beijing 100081, China (e-mail: lelezhang@bit.edu.cn; dengfang@bit.edu.cn; chenjie@bit.edu.cn).

Y. Bi and B. M. Chen are with Department of Electrical and Computer Engineering, National University of Singapore, 117576 Singapore (e-mail: yingcaibi@u.nus.edu; bmchen@nus.edu.sg).

S. K. Phang is with the School of Engineering, Taylor's University, Subang Jaya 47500, Malaysia (e-mail: swee_king@hotmail.com).

X. Chen is with the Temasek Laboratories, National University of Singapore, 117411 Singapore (e-mail: tslcx@nus.edu.sg).

Color versions of one or more of the figures in this paper are available online at <http://ieeexplore.ieee.org>.

Digital Object Identifier 10.1109/TIE.2018.2807401

byproduct of employing these multiple bearing measurements. Specifically, for the estimation of the relative altitude, two kinds of flight scenarios (overflight and loitering) are discussed here. For the overflight scenario, a nonverged stereo geometry [19] can be used directly to compute the relative altitude from two or more images of the GOI taken in distinct viewpoints. Whereas for the loitering scenario, due to the significant yaw-angle measurement bias, it will introduce a large estimation error of the relative altitude by employing the epipolar stereo model [20]. In order to deal with this issue, we propose a technique that utilizes several iterations between the epipolar stereo model and the linear regression model to jointly estimate the relative altitude and yaw-angle measurement bias. Once the heading-measurement bias and the relative altitude are calculated, the target's 3-D localization can be accurately estimated as the target appears in the camera field-of-view. The proposed method can also be applicable to line of sight (LOS) location scenarios, like sound source localization in wireless sensor networks [21].

Thanks to the maneuverability and the simple mechanical configuration of the quadrotor UAV, it has become an increasingly popular topic among researchers and scholars [22]–[24]. In this paper, we use the quadrotor UAV designed by our group as an experimental platform. Particular attention is given to the yaw-angle bias provided in the yaw-angle measurement by the AHRS, where it may vary every time when the AHRS is initialized. Also, the assumption of unknown and constant bias is justified in short instances, as in the case that UAV flying over a ground object.

The main contributions of this paper are as follows.

- 1) The yaw-angle bias and relative altitude between UAV and the target can be jointly estimated in overflight and loitering scenarios using the proposed method.
- 2) Accurate 3-D target geolocation can be realized even if the UAV systems do not meet the aforementioned requirements (georeferenced terrain database and accurate attitude sensors) using the proposed method.

This paper is organized as follows. An overview of the geometry between the UAV and GOI is described in Section II. The estimation of the relative altitude of the UAV above the GOI is discussed in detail in Section III. The target location estimation is introduced in Section IV, followed by the simulation results to evaluate the efficacy of the proposed method. In Section V, the results obtained from the flight test data are presented to verify the method in actual UAV systems implementation. This paper ends with some concluding remarks in the final section.

II. GEOMETRY

The UAV target geolocation model can be visualized in Fig. 1. Mathematically [17], it can be expressed as

$$\begin{aligned} \begin{bmatrix} x_p \\ y_p \end{bmatrix} &= \begin{bmatrix} x_v \\ y_v \end{bmatrix} + \frac{(z_p - z_v)}{(0, 0, 1)C_b^n} \begin{bmatrix} x_f \\ y_f \\ f \end{bmatrix} \\ &\times \begin{bmatrix} 1 & 0 & 0 \\ 0 & 1 & 0 \end{bmatrix} C_b^n \begin{bmatrix} x_f \\ y_f \\ f \end{bmatrix} \end{aligned} \quad (1)$$

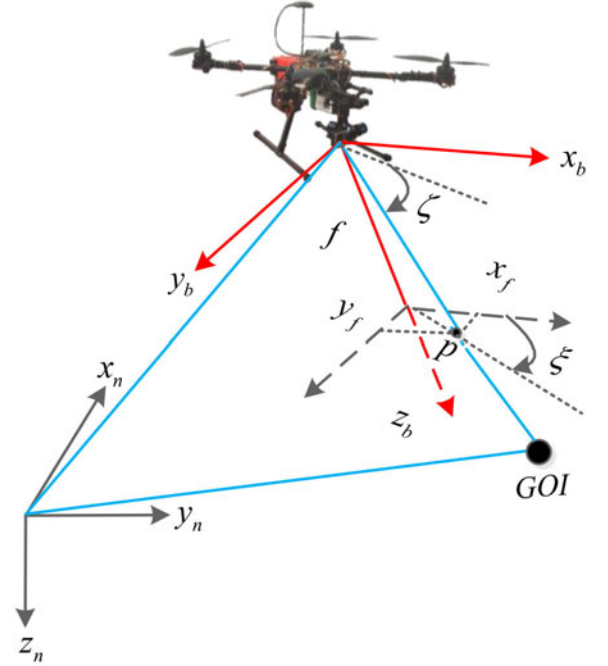


Fig. 1. UAV target geolocation model.

where x_f and y_f are the coordinates of the image of the GOI's corresponding point p in the image plane; $(x_v, y_v, z_v)^T$ and $(x_p, y_p, z_p)^T$ represent the UAV's position and the GOI's position in the navigation frame n , respectively; and f is the focal length of the camera. The UAV navigation state $(x_v, y_v, z_v, \psi, \theta, \phi)$ is measured by the onboard GPS receiver and the AHRS. The rotation matrix C_b^n [25] represents the transformation from the body frame b to the navigation frame n .

The relative altitude between the UAV and GOI, h , is defined by

$$h = z_p - z_v \quad (2)$$

where the estimation of h is shown in Section III.

Generally, in a wing-level flight, the pitch and roll angles of the UAV can be accurately measured, but the yaw-angle measurement is somewhat problematic when a miniaturized magnetic flux gate or a compass is employed as it will introduce large measurement errors. Hence, to facilitate the estimation of the critical yaw-angle bias $\delta\psi$, the pitch and roll measurement errors will be ignored in our studies and only the bias in the yaw angle is considered.

It should be noted that the GOI is identified and is traced from frame to frame using an existing feature-tracking algorithm [26]–[28]. Taking multiple bearing measurements of the GOI ensures that the yaw-angle bias is correctly estimated using the optical method proposed in [17]. The estimation process of the yaw-angle bias $\delta\psi$ is illustrated as follows.

We estimate the parameter $\gamma = [\gamma_1, \gamma_2]^T$, where

$$\gamma_1 := [x_p, y_p]^T$$

is the position of the ground object and

$$\gamma_2 := \delta\psi$$

is the bias error in the attitude-heading measurement provided by the AHRS. The measured variables are

$$y = [y_1, y_2]^T$$

where $y_1 := [x_v, y_v, z_v, x_f, y_f, \theta, \phi]^T$ and $y_2 := \psi$.

From (1), the measurement equation has the general form

$$\gamma_1 = F(y_1, y_2) \quad (3)$$

and the actual measurements are

$$z_1 = y_1 + w_1, w_1 \sim N(0, Q_1) \quad (4)$$

$$z_2 = y_2 + \gamma_2 + w_2, w_2 \sim N(0, Q_2) \quad (5)$$

where the Gaussian measurement noise covariances Q_1 is a 7×7 symmetric positive-definite matrix, and Q_2 is a positive number. Combining (4) and (5) into the measurement equation (3), we obtain the nonlinear measurement equation as follows:

$$\gamma_1 = F(z_1 - w_1, z_2 - (\gamma_2 + w_2)). \quad (6)$$

Using Taylor's theorem then yields the linearized measurement equation

$$F(z_1, z_2) \approx \gamma_1 + \left. \frac{\partial F}{\partial y_2} \right|_{z_1, z_2} \cdot \gamma_2 + \left. \frac{\partial F}{\partial y_1} \right|_{z_1, z_2} \cdot w_1 + \left. \frac{\partial F}{\partial y_2} \right|_{z_1, z_2} \cdot w_2. \quad (7)$$

Suppose that $N(\geq 2)$ bearing measurements of the GOI are taken at the discrete time $k = 1, \dots, N$, that is, $(z_{1_1}, z_{2_1}), \dots, (z_{1_N}, z_{2_N})$, linear regression in the parameter $\gamma \in R^3$ can be formulated by

$$\begin{pmatrix} F(z_{1_1}, z_{2_1}) \\ \vdots \\ F(z_{1_N}, z_{2_N}) \end{pmatrix} = \begin{bmatrix} I_2, & \left. \frac{\partial F}{\partial y_2} \right|_{z_{1_1}, z_{2_1}} \\ \vdots & \vdots \\ I_2, & \left. \frac{\partial F}{\partial y_2} \right|_{z_{1_N}, z_{2_N}} \end{bmatrix} \gamma + W \quad (8)$$

where

$$W \sim N(0, Q)$$

is the equation error with its covariance

$$Q = \text{diag} \left(\left\{ \left(\left. \frac{\partial F}{\partial y_1} \right|_{z_{1_k}, z_{2_k}} \right) Q_1 \left(\left. \frac{\partial F}{\partial y_1} \right|_{z_{1_k}, z_{2_k}} \right)^T + \left(\left. \frac{\partial F}{\partial y_2} \right|_{z_{1_k}, z_{2_k}} \right) Q_2 \left(\left. \frac{\partial F}{\partial y_2} \right|_{z_{1_k}, z_{2_k}} \right)^T \right\}_{k=1}^N \right).$$

From (8), the yaw-angle bias can be solved effectively with the weighted least-square method introduced in [18]. For the estimator, suppose that the weighted matrix $S(2N \times 2N)$ is a diagonal matrix whose elements are the reciprocals of the equation error variances, it [29] proves that the parameter estimate is unbiased estimate with minimum variance.

According to (1), the partial derivatives are obtained by

$$A_k := \left. \frac{\partial F}{\partial y_1} \right|_{z_{1_k}, z_{2_k}}, B_k := \left. \frac{\partial F}{\partial y_2} \right|_{z_{1_k}, z_{2_k}}$$

TABLE I

SCENARIOS CONSIDERED IN THE METHOD

Maneuver	Employed Camera
Overflight	Front
Loitering	Side

and the equation covariance is

$$Q = \text{diag} \left(\{A_k Q_1 A_k^T + B_k Q_2 B_k^T\}_{k=1}^N \right).$$

The parameter estimation is thus given by

$$\hat{\gamma} = \left[\sum_{k=1}^N \begin{bmatrix} I_2 \\ B_k^T \end{bmatrix} (A_k Q_1 A_k^T + B_k Q_2 B_k^T)^{-1} [I_2, B_k] \right]^{-1} \times \sum_{k=1}^N \begin{bmatrix} I_2 \\ B_k^T \end{bmatrix} (A_k Q_1 A_k^T + B_k Q_2 B_k^T)^{-1} F(z_{1_k}, z_{2_k}). \quad (9)$$

III. RELATIVE ALTITUDE ESTIMATION

In this paper, the relative altitude of the UAV above the GOI is estimated by using the stereo vision, rather than measured from a terrain database. Two flight scenarios flown by the UAV are shown in Table I. In these scenarios, a forward-looking and a side-looking camera are mounted on the UAV with depression angle β and with the camera field of view FOV . V represents the UAV's airspeed and f_{GPS} is GPS data acquisition frequency. Details about calculation of the relative altitude in overflight and loitering scenarios are discussed in the following subsections.

A. Overflight

In this scenario, UAV flies in a straight line, while a forward-looking camera looks toward the GOI. In order to estimate the relative altitude h , we use the $N(\geq 2)$ bearing measurements of the GOI introduced in Section II. Specifically, at every discrete time $i (= 1, \dots, N)$, the measurements include the image coordinates of the GOI (x_{f_i}, y_{f_i}) , as well as the current attitude $(\psi_i, \theta_i, \phi_i)$ and position $(x_{v_i}, y_{v_i}, z_{v_i})$ of the UAV are obtained with the onboard sensors.

From [19], the accuracy of the reconstruction from the stereo vision can be enhanced with the improvement of the baseline between the two cameras. However, a longer baseline reduces the number of the bearing measurements available to compute h . A proper threshold value of the baseline distance should be selected to balance and satisfy both requirements.

We set the threshold value of the baseline distance by

$$D_{pt} = l_1 \frac{V}{f_{GPS}} \quad (10)$$

where l_1 is a parameter related to N . Two images are taken as a stereo pair only if the baseline distance T_N between these two corresponding locations for a single camera is larger than the threshold value ($T_N \geq D_{pt}$), as shown in Fig. 2.

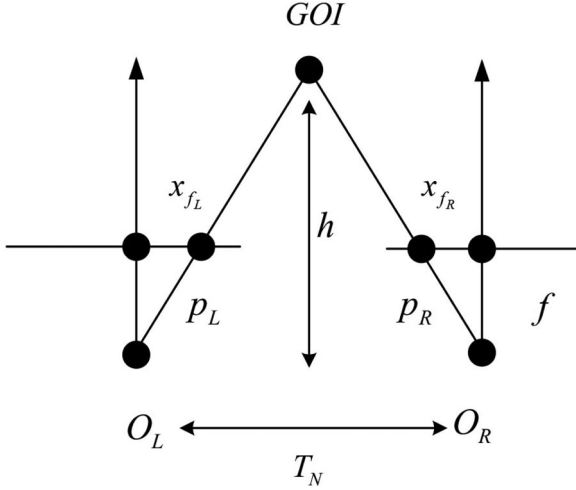


Fig. 2. Nonverged stereo geometry.

In the nonverged geometry, the left and right image plane are coplanar and the optical axes are parallel. The way in which stereo determines the position in space of GOI (see Fig. 2) is triangulation, that is, by intersecting the rays defined by the centers O_L and O_R of projection and the images of GOI, P_L and P_R . Triangulation depends on the solution of the corresponding problem: If (P_L, P_R) is chosen as pairs of corresponding image points, intersecting the rays $O_L P_L$, $O_R P_R$ leads to interpreting the image points as a projection of GOI. In the overflight scenario, the relative altitude of the UAV above the GOI (depth) is estimated from the disparity of corresponding points. That is, given the focal length f of the camera, the relative altitude h can be computed by similar triangles by

$$h = f \frac{T_N}{d} \quad (11)$$

where d is the disparity of corresponding image points (P_L, P_R) , $d = x_{f_R} - x_{f_L}$. Let $P_n = [x_v \ y_v \ z_v]^T$ denote the position of the UAV in the navigation frame n and let $C_n^b = (C_b^n)^T$ denote the rotation transformation from the body frame b to the navigation frame n , and the position $P_b = [x_b \ y_b \ z_b]^T$ of the UAV in the body frame b is calculated as $P_b = (C_b^n)^T P_n$. The distance T_N is computed as $T_N = x_{b_R} - x_{b_L}$.

Any two images from N bearing measurements are used as a stereo pair for every $T \geq D_{pt}$, with a total of m pairs. We then calculate h_j ($j = 1, \dots, m$) by using (11), and the mean of all m pairs, \bar{h} , is regarded as the final relative altitude. Then, inserting calculated \bar{h} into (9), we can estimate the yaw-angle bias $\delta\psi$.

B. Loitering

In this scenario, UAV orbits the GOI and images of the GOI are taken with a side-looking camera. Similar to the overflight scenario, the N bearing measurements of the GOI introduced in Section II are used to estimate the relative altitude h . Again, a threshold value of the baseline arc distance between the two cameras are chosen to balance the stated constraints.

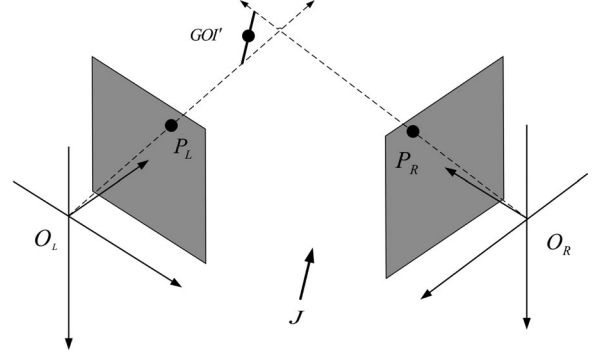


Fig. 3. Epipolar stereo geometry.

We set the threshold value of the baseline arc distance by

$$S_{pt} = l_2 \frac{V}{f_{GPS}} \quad (12)$$

where l_2 is a parameter related to N . Two images are taken as a stereo pair only if the baseline arc distance S between these two corresponding locations is larger than the threshold value ($S \geq S_{pt}$), as shown in Fig. 3. The points P_L and P_R are corresponding image points of the GOI projected in the left and right image frame, along the rays $O_L P_L$ and $O_R P_R$, respectively. We assume that the point GOI is the intersection of the rays $O_L P_L$ and $O_R P_R$. However, since position-measurement and attitude-measurement errors exist in the sensor measurement, the rays will not intersect. The point of intersection can be approximated as the point with minimum distance from the two rays.

Let aP_L ($a \in R$), $T_E + bR^T P_R$ ($b \in R$) be the ray $O_L P_L$ and the ray $O_R P_R$ in the left reference frame, respectively. We denote J as an orthogonal vector with the rays $O_L P_L$ and $O_R P_R$. The translation vector T_E and rotation matrix R define the extrinsic parameters of the stereo cameras. The problem is now simplified to searching the midpoint GOI' of line segment parallel to J that joins $O_L P_L$ and $O_R P_R$.

The endpoints of the line segment ($a_0 P_L$ and $T_E + b_0 R^T P_R$) are calculated to solve the following equation:

$$aP_L - bR^T P_R + c(P_L \times R^T P_R) = T_E \quad (13)$$

for a_0 , b_0 , and c_0 . Thus, the relative altitude h can be expressed as an epipolar stereo model as

$$h = \frac{1}{2} [0 \ 0 \ 1] R_L^T ([1 \ 0 \ 0] M P_L + [0 \ 1 \ 0] M R^T P_R + T_E) \quad (14)$$

where $P_L := [x_{f_L}, y_{f_L}]^T$ and $P_R := [x_{f_R}, y_{f_R}]^T$ are the image coordinates of the corresponding point GOI. T_L , R_L and T_R , R_R are the extrinsic parameters of a stereo pair with respect to the same navigation frame; We have $R = R_R R_L^T$, $T_E = T_L - R^T T_R = R_L(O_R - O_L)$, and $M = [P_L - R^T P_R \ P_L \times R^T P_R]^{-1} T_E$. That is

$$R_L := C_n^b(\psi_L, \theta_L, \phi_L), \quad R_R := C_n^b(\psi_R, \theta_R, \phi_R)$$

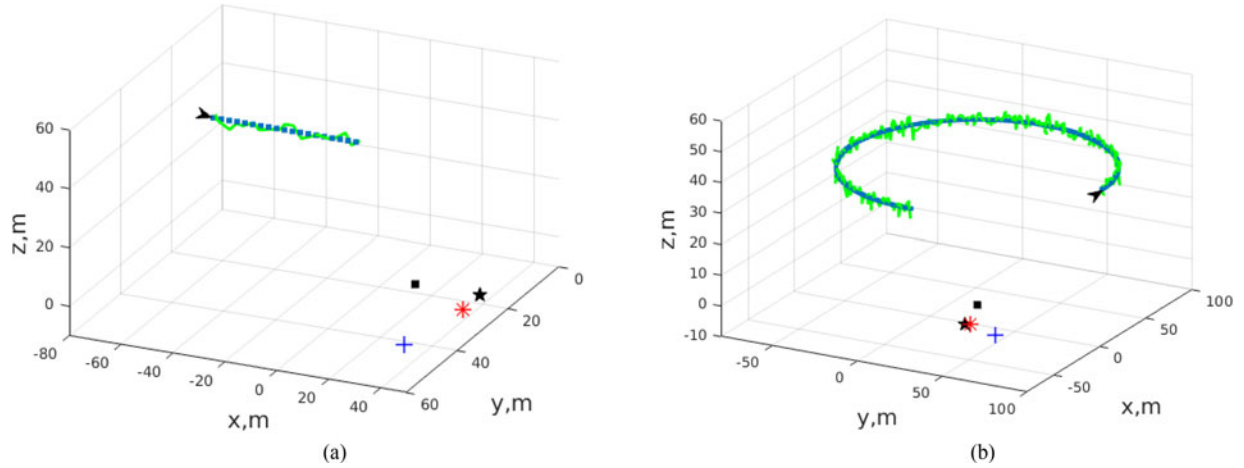


Fig. 4. Single-shot 3-D geolocation of a target for different scenarios. (a) Overflight. (b) Loitering.

TABLE II
SINGLE-SHOT ESTIMATION PERFORMANCE WITH THE USUAL
APPROACH: 100 MC RUNS

Scenario		rms	σ	Max Error
Overflight	x, m	10.04	8.37	20.19
	y, m	25.08	6.52	43.52
Loitering	x, m	11.75	8.16	22.78
	y, m	23.86	6.89	39.02

where $\delta\hat{\psi}$ is estimate of the yaw-angle bias $\delta\psi$ and we set $\psi_L = \psi_i - \delta\hat{\psi}$, $\theta_L = \theta_i$, $\phi_L = \phi_i (1 \leq i < N)$ and $\psi_R = \psi_j - \delta\hat{\psi}$, $\theta_R = \theta_j$, $\phi_R = \phi_j (i < j \leq N)$. Any two images from N bearing measurements are regarded as a stereo pair for every $S \geq S_{pt}$ (on the assumption of m_1 pairs in total) to calculate $h_j (j=1, \dots, m_1)$ by using (14). Then, we can obtain the mean value of m_1 pairs, that is \bar{h} .

As significant heading measurement error occurs in low cost compass, the accuracy of the relative altitude between the UAV and GOI achieved by using (14) is generally poor. Nevertheless, for (9), the estimate of yaw-angle bias hinges on the known relative altitude. We consider several iterations between the epipolar stereo model and linear regression model to jointly estimate the relative altitude and yaw-angle bias. Combining (9) and (14), we can obtain

$$\delta\psi = g(\delta\psi). \quad (15)$$

Giving the initial value $\delta\psi_0$, we employ

$$\delta\psi_{k+1} = g(\delta\psi_k) \quad (16)$$

to generate iterative sequence $\delta\psi_k$. Obviously, if $\delta\psi_k$ converges to $\delta\psi^*$, and $g(\delta\psi)$ is continuous on $\delta\psi^*$, we have

$$\delta\psi^* = \lim_{k \rightarrow \infty} \delta\psi_{k+1} = \lim_{k \rightarrow \infty} g(\delta\psi_k) = g(\delta\psi^*).$$

Then, $\delta\psi^*$ is the solution of (15), and $\delta\psi_k$ can be the approximate solution when k is large enough.

Due to the complexity of (15), there is significant difficulty for formula derivation methods to obtain a simplified form, which is

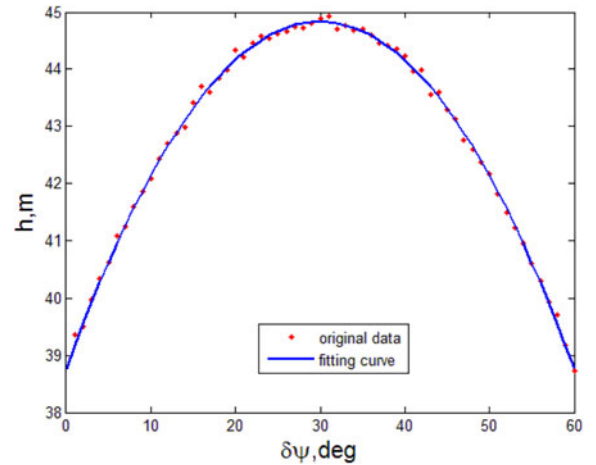


Fig. 5. Fitting curve of $h \sim \delta\psi$.

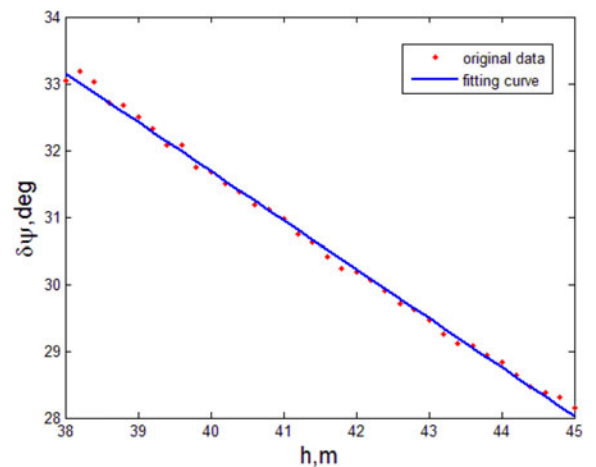


Fig. 6. Fitting curve of $\delta\psi \sim h$.

used to prove the convergence of the iterative algorithm. Therefore, the experimental data produced by (9) and (14) is employed to approximate (15). One point to note is that the experimental data are built on the similar condition as the actual flight test.

TABLE III
 ITERATIVE PROCESS FOR LOITERING SCENARIO

k	0	1	2	3	4
$\delta\psi$, deg	0	2.57	28.17	28.14	28.15

TABLE IV
 RELATIVE ALTITUDE AND YAW-ANGLE BIAS ESTIMATION
 PERFORMANCE: 100 MC RUNS

Scenario		rms	σ	Max Error
Overflight	h, m	0.87	0.79	2.03
	$\delta\psi$, deg	9.92	5.47	18.56
Loitering	h, m	1.03	0.88	2.84
	$\delta\psi$, deg	1.96	0.39	2.99

In most cases, the conclusion of simulation can be applicable to the flight test. Moreover, in the specific scenario presented in this paper, we have obtained a good fitting effect through the least-squares fitting method. But for some data points far away from the fitting curve, probably, these points are coming from different scenarios, and then, we have to refit them and build the new form.

IV. TARGET LOCATION ESTIMATION

Before locating the target, the estimations of the relative altitude \hat{h} and the yaw-angle bias $\delta\hat{\psi}$ are already available using the multiple bearing measurements of the GOI, described in Sections II and III. It should be noted that the relative altitude between the GOI and the target is so small that the GOI's altitude can be approximated as the target's altitude when they are lying on the same ground plane.

For the target geolocation, only one-shot bearing measurement of the target is needed for both the usual approach [13] and our method. The usual approach focuses on calculating the target's two-dimensional (2-D) position $(x_t, y_t)^T$ based on the assumptions that the target's altitude z_t is known and a high-quality AHRS is mounted in the UAV. In this approach, researchers generally did not consider the reduced accuracy of the target geolocation due to the bias in the measurements provided by the low-quality AHRS. On the other hand, the proposed method in this manuscript will provides an accurate 3-D target geolocation even if the sensors accuracy requirements and the target's altitude information are not met. The main idea of our method is that the bias in the yaw-angle measurement $\delta\hat{\psi}$ and the relative altitude \hat{h} are jointly obtained using multiple bearing measurements of the GOI first, and then, the target's 3-D position $(x_t, y_t, z_t)^T$ is given. Once the target is detected, the target corresponding image coordinates $(x_{f_t}, y_{f_t})^T$ will be recorded, and then, the target position in the navigation frame will be obtained. Both the usual method and our proposed method employ (17) and (18) to calculate the target's position. The relationship

TABLE V
 SINGLE SHOT ESTIMATION PERFORMANCE WITH OUR
 METHOD: 100 MC RUNS

Scenario		rms	σ	Max Error
Overflight	x, m	8.55	8.54	30.12
	y, m	9.08	6.40	23.20
	z, m	0.87	0.79	2.03
Loitering	x, m	9.09	9.02	30.02
	y, m	6.22	5.74	14.46
	z, m	1.03	0.88	2.84

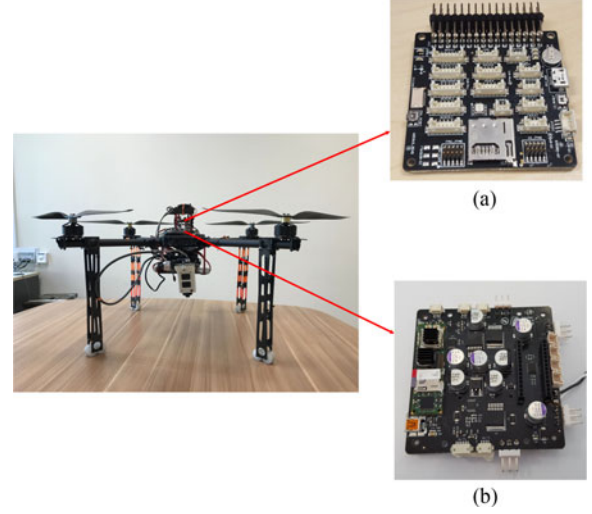


Fig. 7. Quadrotor UAV.

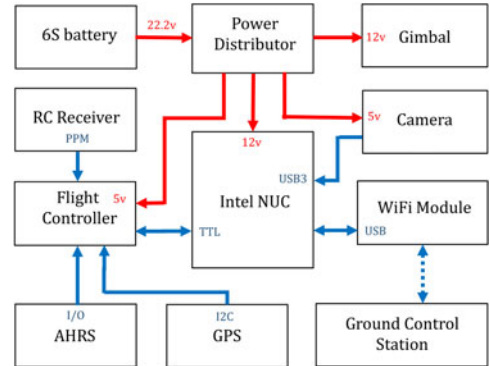


Fig. 8. Hardware integration.

between the target and the UAV state is given by

$$\begin{bmatrix} x_t \\ y_t \end{bmatrix} = \begin{bmatrix} x_v \\ y_v \end{bmatrix} + \frac{\hat{h}}{(0, 0, 1)C_b^n} \begin{bmatrix} x_{f_t} \\ y_{f_t} \\ f \end{bmatrix} \times \begin{bmatrix} 1 & 0 & 0 \\ 0 & 1 & 0 \end{bmatrix} C_b^n \begin{bmatrix} x_{f_t} \\ y_{f_t} \\ f \end{bmatrix} \quad (17)$$

$$z_t = \hat{h} + z_v. \quad (18)$$

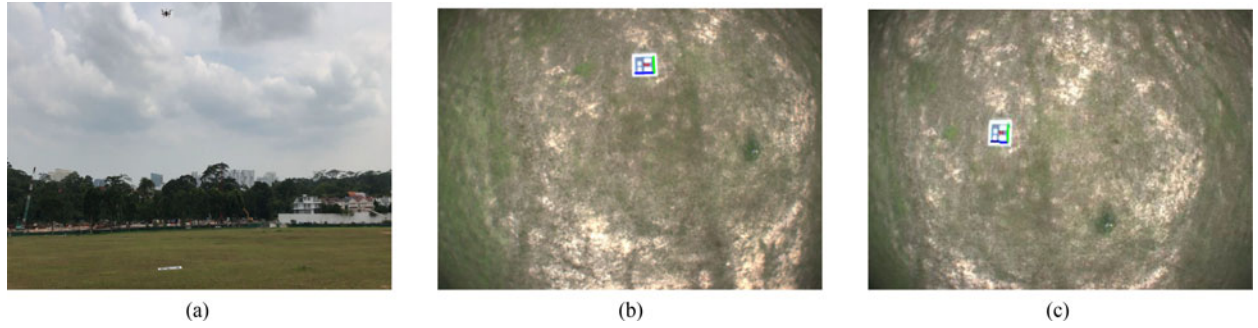


Fig. 9. Flight test: An outdoor scenario. (a) UAV takes visual measurements of the GOI. (b) GOI detection. (c) Target detection.

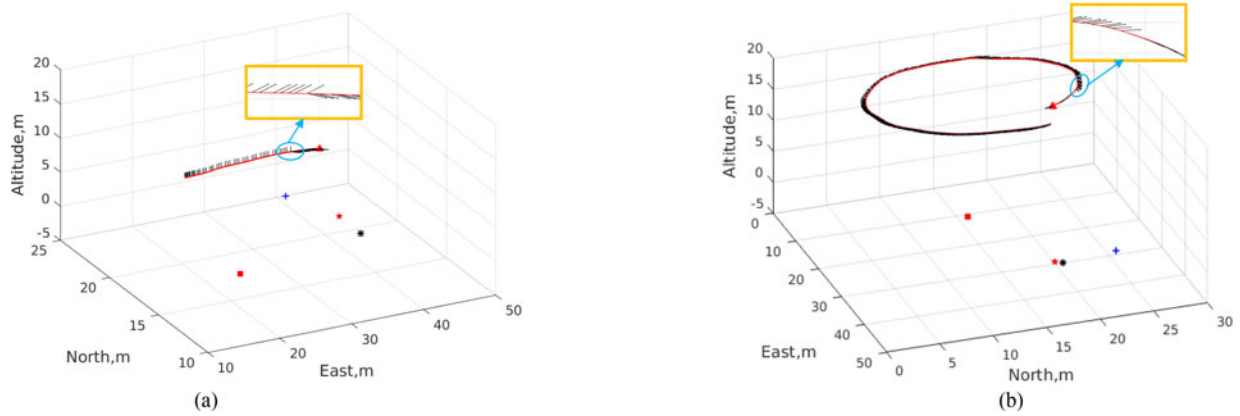


Fig. 10. Target 3-D geolocation. (a) Overflight. (b) Loitering.

For the overflight and loitering scenarios with depression angle $\beta = 45^\circ$ and with the camera field of view $FOV = 30^\circ$, 100 Monte Carlo simulations were run to verify the effectiveness of the proposed method. The measurement process was obtained as follows: constant-altitude flight was $h_a = 45$ m, bias in the yaw-angle measurement was $\delta\psi_a = 30^\circ$, AHRS attitude uncertainty was $\sigma_\psi = \sigma_\theta = \sigma_\phi = 5^\circ$, differential global positioning system (DGPS) horizontal error was $\sigma_x = \sigma_y \approx 0.6$ m, and baroaltitude error was $\sigma_z \approx 1.5$ m. The turn radius was $R = 73$ m, the radian was $\alpha = 1.5\pi$, GPS data acquisition frequency was $f_{GPS} = 4$ Hz, and the UAV's airspeed was $V = 3.44$ m/s.

High level of performance was demonstrated in both overflight and loitering scenarios as presented in Fig. 4, where the blue line is the UAV's GPS actual positions, the green line represents the UAV's GPS measured positions, the solid circle shows the actual position of an GOI measured to estimate the yaw-angle bias, the black star is the target's actual position, the blue cross is the result of the geolocation of the target's position with the usual approach, and the red asterisk represents the result of the geolocation of the target's position with our method.

For state-of-the-art comparison, the usual approach is first simulated. Table II shows the statistical results of the target localization in the north and east direction with the usual approach, in the form of root mean square error (rms), standard deviation (σ), and max error.

We then provide results of target localization using the method proposed in this paper. First, for the overflight scenario, typical runs are presented in Table IV with respect to yaw-angle bias

TABLE VI
TARGET 3-D GEOLOCATION RESULTS WITH THE USUAL APPROACH

	e_x, m	e_y, m
Overflight	3.22	-2.99
Loitering	5.77	-0.55

estimation $\delta\hat{\psi}$ and the relative altitude estimation \hat{h} by setting the parameter $l_1 = \text{int}(\frac{N}{2})$. In Table V, the statistical results are listed associated with the target location in the north, east, and up directions: x , y , and z . Second, for the loitering scenario, the convergence analysis about the estimations is illustrated as follows.

For the aforementioned scenario, herein the proof of its convergence is given as follows. By setting the variables $\delta\psi = 0, 1, \dots, 59, 60^\circ$ and $h = 38.0, 38.2, \dots, 44.8, 45.0$ m and substituting into (14) and (9), respectively, the fitting curves of $h \sim \delta\psi$ and $\delta\psi \sim h$ are obtained as shown in Figs. 5 and 6. The relationship expressions of $h \sim \delta\psi$ and $\delta\psi \sim h$ are approximated as

$$h = -0.0067\delta\psi^2 + 0.4042\delta\psi + 38.7742 \quad (19)$$

$$\delta\psi = -0.7328h + 61.0033. \quad (20)$$

By combining (19) and (20), we obtain

$$\delta\psi = 0.0049\delta\psi^2 - 0.2962\delta\psi + 32.5896. \quad (21)$$

TABLE VII
TARGET 3-D GEOLOCATION RESULTS WITH OUR METHOD

	$T1/s$	$N1$	$\delta\hat{\psi}, \text{deg}$	$\sigma_{\delta\hat{\psi}}, \text{deg}$	\hat{h}, m	$\sigma_{\hat{h}}, m$	e_x, m	e_y, m	e_z, m
Overflight	4.60	47	-38.24	0.78	16.66	0.86	-1.43	1.03	-1.15
Loitering	24.00	242	-24.64	0.16	19.78	0.28	0.67	0.09	-0.36

The derivative of the aforementioned equation is

$$g'(\delta\psi) = 0.0098\delta\psi - 0.2962.$$

Based on Banach's contraction mapping principle, the convergence of the fixed-point iterative method is described in [31].

Theorem 4.1: Let $g(\delta\psi)$ satisfy the following requirements in the interval $[a, b]$.

- 1) For each $\delta\psi \in [a, b]$, $g(\delta\psi) \in [a, b]$.
- 2) There exists $0 < L < 1$, for each $\delta\psi \in [a, b]$, $|g'(\delta\psi)| \leq L$.

Then, (15) in the interval $[a, b]$ has unique solution $\delta\psi^*$. Moreover, for each $\delta\psi_0 \in [a, b]$, iterative sequence

$$\delta\psi_{k+1} = g(\delta\psi_k) \quad (k = 0, 1, 2, \dots)$$

converges to $\delta\psi^*$, and

$$|\delta\psi^* - \delta\psi_k| \leq \frac{L^n}{1 - L} |\delta\psi_1 - \delta\psi_0|.$$

According to Theorem 4.1, its convergence can be guaranteed by setting the parameters $\delta\psi \in [0, 60]$, $\delta\psi_0 = 0$, $k = 4$, and $L = 0.9$. The iterative process for the loitering scenario is illustrated in Table III. The statistical results for the loitering scenario are listed in Tables IV and V.

The statistical results verify the method described in this paper. Compared with the usual approach, we can see that the horizontal target position error is reduced by 14.54 and 15.58 m, while the vertical target position error is 0.87 and 1.03 m for the overflight and loitering scenario, respectively.

V. ACTUAL FLIGHT RESULTS

The quadrotor UAV used in this flight test is a laboratory product designed by our group as shown in Fig. 7. It was especially catered to carry high payload (> 2 kg) with a long-endurance flight (> 20 min). The UAV has the ability to fly on predefined waypoint and circular path autonomously, so it can be used as a test platform to validate our method.

The hardware integration is described in Fig. 8. The UAV is equipped with a power distributor, a flight controller, an onboard computer, and a gimbal-controlled camera. The power distributor outputs 12 and 5 V for all sorts of electronics. The flight controller provides the control input based on the guidance law and AHRS information. Fig. 7(a) and 7(b) shows the flight controller and power distributor, respectively. An Intel NUC minicomputer is selected as an onboard computer and mounted in the UAV. It is run in the ROS system [32], where it enables image processing and trajectory planning in the real-time during flight. A monocular camera, PointGrey BlackFly is used for visual measurements during the flight. The camera is set to point directly downwards at the GOI. The pan-tilt gimbal is employed

to handle the stabilization and direction of the camera, as shown in Fig. 7.

The proposed method in previous sections is verified through actual flight data using the quadrotor UAV. In our implementation, the full algorithm is able to run with 18 Hz in our onboard NUC, which is more than sufficient for any real-time application. The flight test in an outdoor environment is presented in Fig. 9. The quadrotor UAV is flying two different paths corresponding to overflight and loitering scenarios described in Section IV. The UAV is commanded to fly these paths as shown in Fig. 10. The red path represents the actual position measurements of the UAV measured by the DGPS. The arrows along the path represent the yaw angle measured by the AHRS. The red square and red star are the ground truths provided by the DGPS for the positions of the GOI and the target, respectively. The triangle is the UAV's position, where the target is detected in the image. For each path, there are two stages: calibration stage and geolocation stage. The calibration stage refers that the UAV relies on feature detection to take multiple measurements of the GOI to obtain the estimation of the yaw-angle bias and the relative altitude, shown as the line segments with significant angular offset between the direction of motion and the arrows in Fig. 10. The geolocation stage is the rest of the path where the UAV first searches the target, and then, locate it once detected. The blue cross and the black asterisk represent the results of target geolocation using the usual approach and our method, respectively. In order to identify the GOI and the target easily, one AprilTag marker [33], [34] is used as the GOI and another AprilTag is mounted on the target. It should be noted that not all features provided by the AprilTag marker are employed for this experiment but only the pixel position of the center point of the AprilTag marker.

The following assumptions in the measurement process are used: $\sigma_x = \sigma_y = 0.2$ m, $\sigma_z = 1$ m, $\sigma_\psi = \sigma_\theta = \sigma_\varphi = 1^\circ$, and $\sigma_\xi = \sigma_\zeta = 0.5^\circ$.

The assumption of the constant bias in the yaw-angle measurement is justified according to Fig. 10. Before eliminating the bias, the arrows show significant angular offset with respect to the direction of motion. After having an estimate of the yaw-angle bias, the angular offset decreases. The main result is that the bias in the yaw-angle measurement and the relative altitude can be jointly and accurately estimated using the multiple bearing measurements of the GOI. As a result, the 3-D geolocation of the target was realized.

For these two scenarios, the localization errors of the target in the north and east direction using the usual approach are listed in Table VI. Also, the estimations of the bias in the yaw-angle measurement and the relative altitude, and the localization errors of the target in the north, east, and up direction using our method are reported in Table VII, where $T1$ represents the length of the

video record selected with $N1$ frames/data points available, in which the GOI is tracked frame by frame.

The test results validate the effectiveness of our method where the horizontal target position error is reduced by 2.63 and 5.12 m in comparison with the usual approach, at the same time, the vertical target position error is 1.15 and 0.36 m for the overflight and loitering scenario, respectively.

VI. CONCLUSION

A novel vision-based geolocation method of determining the target's 3-D position was developed in this paper, with the consideration of the low-quality AHRS onboard UAV. The usual methods to target geolocation had to rely on many requirements (i.e., georeferenced terrain database and accurate attitude sensors). Therefore, the geolocation of the target cannot be realized if the UAV systems do not meet these requirements. In contrast, the geolocation method proposed in this paper only uses the computer vision technique to provide accurate estimations of the target's altitude and yaw-angle measurement bias. The contribution of the method is to remove these requirements in current systems while maintaining high target location accuracy.

The performance of this geolocation method was evaluated by the actual flight test. The results show that the method provides the accurate joint estimation of the relative altitude and yaw-angle measurement bias using multiple bearing measurements of a GOI for the overflight and loitering scenario, respectively. Finally, the target 3-D position is accurately calculated using only one-shot measurement. Compared with the usual approach, the position uncertainty using this method is decreased by about 5 m in the horizontal direction, while the achieved position accuracy using this method is about 0.5 m in the vertical direction.

For generality of the proposed method, future work will address moving GOI scenarios and also geolocating and tracking a moving target.

REFERENCES

- [1] D. J. Pack, G. W. P. York, R. E. Sward, and S. D. Cooper, "Searching, detecting, and monitoring emergency sites using multiple unmanned aerial vehicles," in *Proc. AIAA*, Sep. 2005, pp. 2005–7031.
- [2] B. Grocholsky, S. Bayraktar, V. Kumar, and G. Pappas, "UAV and UGV collaboration for active ground feature search and localization," in *Proc. AIAA*, Sep. 2004, pp. 2004–6565.
- [3] J. E. Gomez-Balderas, G. Flores, L. G. Carrillo, and R. Lozano, "Tracking a ground moving target with a quadrotor using switching control," *J. Intell. Robot. Syst.*, vol. 70, no. 1, pp. 65–78, Apr. 2013.
- [4] S. Minaeian, J. Liu, and Y. Zhong, "Vision-based target detection and localization via a team of cooperative UAV and UGVs," *IEEE Trans. Syst., Man, Cybern., Syst.*, vol. 46, no. 7, pp. 1005–1016, Jul. 2016.
- [5] C. Kanellakis and G. Nikolakopoulos, "Survey on computer vision for UAVs: Current developments and trends," *J. Intell. Robot. Syst.*, vol. 87, no. 1, pp. 141–168, Jul. 2017.
- [6] S. Y. Zhao, Z. Y. Hu, B. M. Chen, and T. H. Lee, "A robust real-time vision system for autonomous cargo transfer by an unmanned helicopter," *IEEE Trans. Ind. Electron.*, vol. 62, no. 2, pp. 1210–1218, Feb. 2015.
- [7] F. Lin, X. Dong, B. M. Chen, K. Lum, and T. H. Lee, "A robust real-time embedded vision system on an unmanned rotorcraft for ground target following," *IEEE Trans. Ind. Electron.*, vol. 59, no. 2, pp. 1038–1049, Feb. 2012.
- [8] X. Zhang, B. Xian, B. Zhao, and Y. Zhang, "Autonomous flight control of a nano quadrotor helicopter in a GPS-denied environment using on-board vision," *IEEE Trans. Ind. Electron.*, vol. 62, no. 10, pp. 6392–6403, Oct. 2015.
- [9] Q. Fu, Q. Quan, and K. Y. Cai, "Robust pose estimation for multirotor UAVs using off-board monocular vision," *IEEE Trans. Ind. Electron.*, vol. 64, no. 10, pp. 7942–7951, Oct. 2017.
- [10] L. Wang and Z. J. Zhang, "Automatic detection of wind turbine blade surface cracks based on UAV-taken images," *IEEE Trans. Ind. Electron.*, vol. 64, no. 9, pp. 7293–7303, Sep. 2015.
- [11] I. H. Wang, V. N. Dobrokhodov, I. I. Kaminer, and K. D. Jones, "On vision-based target tracking and range estimation for small UAVs," in *Proc. AIAA*, 2005, pp. 2005–6401.
- [12] V. N. Dobrokhodov, I. I. Kaminer, K. D. Jones, and R. Ghabcheloo, "Vision-based tracking and motion estimation for moving targets using small UAVs," in *Proc. Amer. Control Conf.*, Minneapolis, MN, USA, Jun. 2006, pp. 1–6.
- [13] V. N. Dobrokhodov, I. I. Kaminer, K. D. Jones, and R. Ghabcheloo, "Vision-based tracking and motion estimation for moving targets using unmanned air vehicles," *J. Guid. Control Dyn.*, vol. 31, no. 4, pp. 907–917, Jul. 2008.
- [14] D. B. Barber, J. D. Redding, T. W. McLain, R. W. Beard, and C. N. Taylor, "Vision-based target geolocation using a fixed-wing miniature air vehicle," *J. Intell. Robot. Syst.*, vol. 47, no. 4, pp. 361–382, Dec. 2006.
- [15] M. E. Campbell and M. Wheeler, "Vision-based geolocation tracking system for uninhabited aerial vehicles," *J. Guid. Control Dyn.*, vol. 33, no. 2, pp. 521–532, Mar. 2010.
- [16] H. K. Min, and G. N. DeSouza, "Geolocation of multiple targets from airborne video without terrain data," *J. Intell. Robot. Syst.*, vol. 62, no. 1, pp. 159–183, Apr. 2011.
- [17] M. Pachter, N. Ceccarelli, and P. R. Chandler, "Vision-based target geolocation using micro air vehicles," *J. Guid. Control Dyn.*, vol. 31, no. 3, pp. 597–615, 2008.
- [18] N. R. Draper and H. Smith, *Applied Regression Analysis*. New York, NY, USA: Wiley-Interscience, 1998, pp. 108–111.
- [19] M. Z. Brown, D. Burschka, and G. D. Hager, "Advances in computational stereo," *IEEE Trans. Pattern Anal. Mach. Intell.*, vol. 25, no. 8, pp. 993–1008, Aug. 2003.
- [20] E. Trucco and A. Verri, *Introductory Techniques for 3-D Computer Vision*. Englewood Cliffs, NJ, USA: Prentice-Hall, 1998, pp. 150–170.
- [21] F. Deng *et al.*, "Energy-based sound source localization with low power consumption in wireless sensor networks," *IEEE Trans. Ind. Electron.*, vol. 64, no. 6, pp. 4894–4902, Jan. 2017.
- [22] F. Y. Chen, R. Q. Jiang, K. K. Zhang, B. Jiang, and G. Tao, "Robust backstepping sliding-mode control and observer-based fault estimation for a quadrotor UAV," *IEEE Trans. Ind. Electron.*, vol. 63, no. 8, pp. 5044–5055, Aug. 2016.
- [23] H. Liu, J. X. Xi, and Y. S. Zhong, "Robust attitude stabilization for non-linear quadrotor systems with uncertainties and delays," *IEEE Trans. Ind. Electron.*, vol. 64, no. 7, pp. 5585–5594, Jul. 2017.
- [24] B. L. Tian, L. H. Liu, H. C. Lu, Z. Y. Zuo, Q. Zong, and Y. P. Zhang, "Multivariable finite time attitude control for quadrotor UAV: Theory and experimentation," *IEEE Trans. Ind. Electron.*, vol. 65, no. 3, pp. 2567–2577, Mar. 2018.
- [25] D. H. Titterton and J. L. Weston, *Strapdown Inertial Navigation Technology*. Stevenage, U.K.: Inst. of Elect. Eng., 2004, pp. 17–55.
- [26] D. G. Lowe, "Distinctive image features from scale-invariant keypoints," *Int. J. Comput. Vis.*, vol. 60, no. 2, pp. 91–110, Nov. 2004.
- [27] H. Bay, A. Ess, T. Tuytelaars, and L. V. Gool, "Surf: Speeded up robust features," in *Proc. Eur. Conf. Comput. Vis.*, Graz, Austria, May 2006, pp. 404–417.
- [28] E. Rublee, V. Rabaud, K. Konolige, and G. Bradski, "ORB: An efficient alternative to SIFT or SURF," in *Proc. IEEE Int. Conf. Comput. Vis.*, Barcelona, Spain, Nov. 2011, pp. 2564–2571.
- [29] R. L. Plackett, "A historical note on the method of least squares," *Biometrika*, vol. 36, no. 3/4, pp. 458–460, Dec. 1949.
- [30] O. Faugeras, *Three-Dimensional Computer Vision: A Geometric Viewpoint*. Cambridge, MA, USA: MIT Press, 1993, pp. 165–230.
- [31] L. J. Ding and Q. Y. Chen, *Numerical Analysis Methods*, 2nd ed. Beijing, China: Beijing Inst. of Technol. Press, 2008.
- [32] M. Quigley *et al.*, "ROS: An open-source robot operating system," in *Proc. ICRA Workshop Open Source Softw.*, Kobe, Japan, 2009.
- [33] E. Olson, "AprilTag: A robust and flexible visual fiducial system," in *Proc. IEEE Int. Conf. Robot. Autom.*, Shanghai, China, May. 2011, pp. 3400–3407.
- [34] J. Wang and E. Olson, "AprilTag 2: Efficient and robust fiducial detection," in *Proc. IEEE/RSJ Int. Conf. Intell. Robot. Syst.*, Daejeon, Korea, Oct. 2016, pp. 4193–4198.



Lele Zhang received the B. E. degree in automation from Inner Mongolia University, Hohhot, China, in 2013. He is currently working toward the Ph.D. degree in control science and engineering with the School of Automation, Beijing Institute of Technology, Beijing, China.

He was involved in research work as a Visiting Ph.D. Student with the Department of Electrical and Computer Engineering, National University of Singapore, from November 2016 to November 2017. His current research interests include camera calibration, simultaneous localization and mapping (SLAM), and deep learning, specifically in the area of aerial robotics.



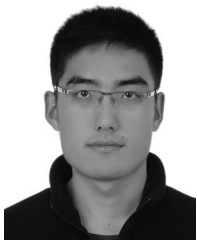
Fang Deng (M'15) received the B. E. and Ph.D. degrees in control science and engineering from the Beijing Institute of Technology, Beijing, China, in 2004 and 2009, respectively.

He is currently an Associate Professor with the School of Automation, Beijing Institute of Technology. His research interests include intelligent fire control, intelligent information processing, and smart wearable devices.



Jie Chen (SM'12) received the B.S., M.S., and Ph.D. degrees in control science and engineering from the Beijing Institute of Technology, Beijing, China, in 1986, 1996, and 2001, respectively.

He is currently a Professor with the School of Automation, Beijing Institute of Technology. His current research interests include complex systems, multiagent systems, multiobjective optimization and decision, constrained nonlinear control, and optimization methods.



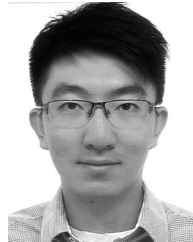
Yingcai Bi received the Bachelor's degree in automation engineering from the Nanjing University of Aeronautics and Astronautics, Nanjing, China, in 2011, and the Master's degree in control science and engineering from Beihang University, Beijing, China, in 2014. He is currently working toward the Ph.D. degree in electrical and computer engineering with the NUS Graduate School for Integrative Sciences and Engineering, National University of Singapore, Singapore.

His research interests include multisensor fusion, visual-inertial odometry, and SLAM, specifically in the area of micro aerial vehicle.



Swee King Phang (M'14) received the B.Eng. and Ph.D. degrees in electrical engineering from the National University of Singapore, Singapore, in 2010 and 2014, respectively.

He is currently a Lecturer with Taylor's University, Subang Jaya, Malaysia. His research interests include system and control of unmanned aerial systems (UASs), including modeling and flight controller design of the UAS, indoor navigation of the UAS, and trajectory optimization.



Xudong Chen received the B.Eng. degree in mechanical engineering from the National University of Singapore (NUS), Singapore, in 2015, where he is currently working toward the Master's degree in electrical engineering.

He is currently an Associate Scientist with the Control Science Group, Temasek Laboratories, NUS. His research interests include autonomous system localization and navigation, control and sensor fusion, computer vision, and deep learning.



Ben M. Chen (S'89–M'92–SM'00–F'07) received the B.S. degree in mathematics from Xiamen University, Xiamen, Fujian, China, in 1983, the M.S. degree in electrical engineering from Gonzaga University, Spokane, WA, USA, in 1988, and the Ph.D. degree in electrical and computer engineering from Washington State University, Pullman, WA, USA, in 1991. He is currently a Professor and Provost's Chair with the Department of Electrical and Computer Engineering, National University of Singapore,

Singapore, where he is also serving as the Director of the Control, Intelligent Systems and Robotics Group. He has authored a dozen research monographs including *Robust and H_∞ Control* (Springer, New York, 2000), *Hard Disk Drive Servo Systems* (Springer, 1st Edition, 2002 and 2nd Edition, 2006), *Linear Systems Theory* (Birkhäuser, Boston, MA, USA, 2004), *Unmanned Rotorcraft Systems* (Springer, New York, NY, USA, 2011), and *Stock Market Modeling and Forecasting* (Springer, New York, NY, USA, 2013). His current research interests include unmanned systems, robust control, control applications, and financial market modeling.

Prof. Chen had served on the editorial boards of several international journals including the IEEE TRANSACTIONS ON AUTOMATIC CONTROL, SYSTEMS & CONTROL LETTERS, and *Automatica*. He currently serves as an Editor-in-Chief for *Unmanned Systems*.